OUKA
Osaka University Knowledge Archive

Title	Kinetics of denaturation and renaturation processes of double-stranded helical polysaccharide, xanthan in aqueous sodium chloride
Author(s)	Tomofuji, Yu; Matsuo, Koichi; Terao, Ken
Citation	Carbohydrate Polymers. 275 p.118681
Issue Date	2021-09-21
oaire:version	AM
URL	https://hdl.handle.net/11094/84559
rights	© 2021. This manuscript version is made available under the CC-BY-NC-ND 4.0 license.
Note	

Osaka University Knowledge Archive : OUKA

https://ir.library.osaka-u.ac.jp/

Osaka University

Kinetics of denaturation and renaturation processes of double-stranded helical polysaccharide, xanthan in aqueous sodium chloride

Yu Tomofuji[a], Koichi Matsuo[b], and Ken Terao[a]*

[a] *Department of Macromolecular Science, Graduate School of Science, Osaka University, 1-1, Machikaneyama-cho, Toyonaka, Osaka 560-0043, Japan*

[b] *Hiroshima Synchrotron Radiation Center, Hiroshima University, Kagamiyama, Higashi-hiroshima, Hiroshima 739-0046, Japan*

* Corresponding author.

Phone: +81-6-6850-5459

E-mail addresses: tomofujiy16@chem.sci.osaka-u.ac.jp (Y. Tomofuji); pika@hiroshima-u.ac.jp (K. Matsuo); kterao@chem.sci.osaka-u.ac.jp (K. Terao).

ABSTRACT

Circular dichroism (CD) and small-angle X-ray scattering (SAXS) measurements were made for three xanthan samples, a double helical polysaccharide, in 5 or 10 mM aqueous NaCl after rapid temperature change to investigate the kinetics of the conformational change between the ordered and disordered states. After the rapid heating, the CD signal mainly reflecting the carbonyl groups on the side chains quickly changed (< 150 s) while the scattering intensity from SAXS around q (magnitude of the scattering vector) = 1 nm^{-1} changed more gradually, reflecting the main-chain conformation. The difference between CD and SAXS implies us the intermediate conformation which can be regarded as a loose double helix. The SAXS profile in the rapid cooling process showed that the loose double helical structure was constructed within 150 s, but the CD signal slowly changed with around 2 days to recover the native tight double helix.

Keywords: double helix; conformational change; small-angle X-ray scattering; circular dichroism; intermediate state

Abbreviations: c, polymer mass concentration; c_d, denatured concentration; CD, circular dichroism; C_s, salt concentration; d, bead diameter; $Đ$, dispersity index; L, contour length; L_w, weight-average contour length; L_k, Kuhn segment length; k, first-order rate constant; K, optical constant; MALS, multi-angle light scattering; M_L, molar mass per unit contour length; M_n, number-average molar mass; M_w, weight-average molar mass; PEO, polyethylene oxide; $P(q)$, form factor; q, magnitude of the scattering vector; R_g, radius of gyration; RI, refractive index; R_q, Rayleigh ratio; SAXS, small-angle X-ray scattering; SEC, size-exclusion chromatography; $S(q)$, structure factor; t, time; V_e, retention volume; v_p, partial specific volume; z, number of moles of electron per unit mass of the solute; $\rho_{e,s}$, electron density of the solvent; $\Delta I(q)$, excess scattering intensity; η_{sp}, specific viscosity; $[\theta']$, specific ellipticity; λ_0, wavelength in a vacuum; $\partial n/\partial c$, refractive index increment.

1. Introduction

Xanthan or xanthan gum, for which representative chemical structure is shown in Fig. 1 but the actual chemical structure varies (Kool, Gruppen, Sworn, & Schols, 2013), is an extracellular polysaccharide. It has multiple anionic groups on each side chain. Xanthan is therefore well soluble both in water and saline. It is widely used for food additives (Hublik, 2012; Nishinari, Turcanu, Nakauma, & Fang, 2019) and biomedical applications (Kumar, Rao, & Han, 2018) because dilute solution of xanthan has significantly high viscosity. Since the rheological properties of xanthan in aqueous media are substantially influenced by the chain conformation, its dimensional, hydrodynamic, spectroscopic, and thermodynamic properties have been widely investigated (Dalheim, Christensen, Comesse, & Renou, 2020; Morris, 2019; Rinaudo, 2008; Sato & Matsuda, 2009) to clarify the conformational properties in solution. Even though the main chain of xanthan consists of β-1,4-glucan, xanthan can form antiparallel double helix in the crystal (Okuyama et al., 1980). The double helical chains were also found in the electron micrograph (Stokke, Elgsaeter, & Smidsrod, 1986; Stokke, Smidsrød, & Elgsaeter, 1989) and the atomic force micrograph (Camesano & Wilkinson, 2001; Capron, Alexandre, & Muller, 1998; Moffat, Morris, Al-Assaf, & Gunning, 2016). One of the representative characteristics of xanthan is that the double helical structure can exist in the aqueous media. The double helical xanthan transforms to the single disordered chain in a low ionic strength aqueous solution with raising temperature (Kitamura, Takeo, Kuge, & Stokke, 1991; Liu & Norisuye, 1988a, 1988b; Liu, Sato, Norisuye, & Fujita, 1987). The ordered double helical structure has significantly high chain stiffness, for which Kuhn's segment length L_k was estimated to be 240 ± 40 nm (Sato, Norisuye, & Fujita, 1984a) in terms of the wormlike chain model (Kratky & Porod, 1949; Yamakawa & Yoshizaki, 2016). This value is much larger than the disordered xanthan (L_k = 42 nm) (Liu et al., 1987). Furthermore, the double-helical hairpin like conformation can be formed in the renatured process on the basis of the molar mass and the intrinsic viscosity in aqueous NaCl (Capron, Brigand, & Muller, 1997). This hairpin like conformation can also be found by the microscopic observations (Capron et al., 1998; Moffat et al., 2016; Stokke et al., 1989). Furthermore, more complicated aggregates are found by means of light scattering (Matsuda, Biyajima, & Sato, 2009; Matsuda, Okumura, & Tasaka, 2018; Matsuda, Sugiura, Okumura, & Tasaka, 2016; Merino-González & Kozina, 2017; Papagiannopoulos, Sotiropoulos, & Radulescu, 2016) and atomic force microscopy (Ikeda, Gohtani, Nishinari, & Zhong, 2012; Matsuda, Sugiura, Mays, & Tasaka, 2015; Teckentrup et al., 2017) depending on the renatured condition. The resulting conformation influences their rheological behaviors (Choppe, Puaud, Nicolai, & Benyahia, 2010; Oviatt & Brant, 1994; Papagiannopoulos, Sotiropoulos, & Pispas, 2016). Conformational change of xanthan has also recently been studied by some modern method with continuous change of ionic strength (Savi, de Freitas, Sassaki, Koop, & Silveira, 2015) and the combination of viscosity and infrared absorption at low salt concentrations (Brunchi, Avadanei, Bercea, & Morariu, 2019).

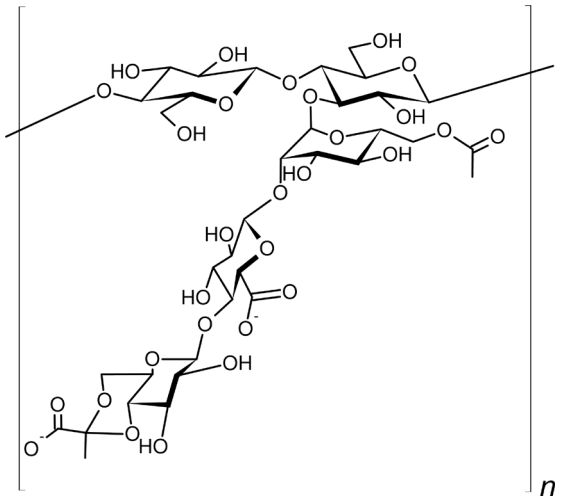

Fig. 1. Chemical structure of xanthan.

The kinetics of the conformational change may be an important research topic taking again into consideration that the obtained renatured conformation can be controllable by the solvent and temperature condition in the denature-renature processes. Indeed, optical rotation after abrupt change of the salt concentration revealed that the renature process was the first order reaction (Norton, Goodall, Frangou, Morris, & Rees, 1984; Norton, Goodall, Morris, & Rees, 1980). More recently, relatively slow change of the viscoelasticity was found after abrupt temperature changes (Bercea & Morariu, 2020). However, kinetics of formation and deformation of the double stranded conformation has not been fully understood.

Recent development of synchrotron-radiation X-ray sources and detectors allows us to make time-resolved small-angle X-ray scattering (SAXS) measurement with high accuracy (Otsubo & Terao, 2021). Analyses of the SAXS data yield the content of the double stranded conformation which cannot be observed in the previous studies because circular dichroism (CD) and optical rotation can be affected by the side chain conformation and rheological data reflects the intermolecular association and entanglement. In this study, we therefore attempted to make both time-resolved SAXS and CD measurements for relatively low molar mass xanthan for which weight-average molar mass M_w ranges between 300 and 500 kg mol^{-1} after rapid temperature change to clarify the kinetics of the temperature-induced conformational change. Synchrotron radiation CD measurements in the wavelength range down to the ultraviolet region were also examined to explore the local conformation after the abrupt temperature change.

2. Materials & methods

2.1. Xanthan samples and their characterization

Three low molar mass xanthan samples were prepared in the following manner. A xanthan sample (TCI, Tokyo, Japan) was dissolved in 100 mM aqueous NaCl to obtain the solution with the polymer mass concentration c = 10 mg mL^{-1}. The solution was sonicated with a Branson Sonifier Advanced 450 (20 kHz) in an ice bath for 6 h to reduce the chain length. The resultant solution was poured into a large amount of acetone to precipitate the xanthan sample. The obtained sample was designated as **X461k**. This xanthan sample was further purified by the fractional precipitation with 100 mM aqueous NaCl as a solvent and acetone as a precipitant after the counter ion was completely changed to sodium in the manner reported previously (Sato, Norisuye, & Fujita, 1984b). The appropriate middle fractions, **X341k** and **X400k**, were also chosen for this study. ^{1}H

NMR measurements were examined for the D_2O solution of **X341k** to determine the acetate/pyruvate ratio as 1.5 with the literature method (Brunchi et al., 2019).

Size-exclusion chromatography (SEC) equipped with a multi-angle light scattering photometer (MALS) and a differential refractive index (RI) detector was carried out for the three samples in aqueous NaCl with the salt concentration C_s = 100 mM to determine M_w, the radius of gyration R_g, and the dispersity index $Đ$ defined as the ratio of M_w to the number-average molar mass M_n. A GPC-101 chromatography system (Shodex, Japan), a DAWN HELEOS II MALS detector (Wyatt technology Co., USA, the wavelength λ_0 in a vacuum was 658 nm), and a RI detector were used with serially connected SEC columns, that is, a guard column (OHpak SB-G, Showa Denko) and two SEC columns (OHpak SB-806M-HQ, Showa Denko) set in a column oven at 40 °C. The universal calibration method (Grubisic, Rempp, & Benoit, 1967; Pasch, 2012) was also applied for the RI chromatogram to confirm the validity of M_w with the standard polyethylene oxide (PEO) samples (Tosoh, Japan) ranging in M_w from 24 to 790 kg mol^{-1}; the literature relationship between the intrinsic viscosity and M_w for PEO (Kawaguchi, Imai, Suzuki, Miyahara, & Kitano, 1997) and for xanthan (Sato, Kojima, Norisuye, & Fujita, 1984) were utilized to calculate molar mass at each elution volume. The SEC-MALS measurement was also made for the solution treated at 85 °C for 30 min and at 20 °C for 48 h in 5 or 10 mM aqueous NaCl with the denatured concentration c_d of about 3 or 6 mg mL^{-1} to estimate the molecular characteristics of renatured samples. The column temperature was set to be 30 °C. The refractive index increment $\partial n/\partial c$ at λ_0 = 658 nm was estimated from the literature values (Liu et al., 1987; Sato, Norisuye, et al., 1984b) in 10 and 100 mM aqueous NaCl. The $\partial n/\partial c$ value in 5 mM aqueous NaCl was assumed to the same as that at C_s = 10 mM because of substantially no C_s dependence of $\partial n/\partial c$.

Aqueous NaCl with C_s = 5 and 10 mM was chosen as the solvents for the following SAXS, CD, and viscosity measurements. Each xanthan sample was dried in a vacuum at least 12 hours before solution preparation. Polymer mass concentration c of xanthan was determined from the weight ratio of xanthan to the solution with the solvent density.

2.2. Circular dichroism

CD measurement was performed for the three xanthan samples in 5 mM and 10 mM aqueous NaCl with the CD spectropolarimeter of BL-12 in HiSOR (Hiroshima, Japan) for which details are available elsewhere (Matsuo & Gekko, 2013) and/or a Jasco J720WO spectropolarimeter to determine the specific ellipticity [θ'], the ellipticity divided by the path length and c. A specially designed cell with CaF_2 windows (Matsuo, Sakai, Matsushima, Fukuyama, & Gekko, 2003) was used for the former equipment to evaluate the ellipticity down to λ_0 = 180 nm. The path length was set as 0.1 mm with an appropriate spacer. Two rectangular quartz cells with the path lengths of 2 or 5 mm were used for the latter equipment. For the rapid temperature change experiment, we installed the cell into the cell holder controlled at target temperature. Temperature inside the cell became the targeted temperature within 150 s for the apparatuses.

2.3. Small-angle X-ray scattering

SAXS measurements with rapid temperature change were carried out at the BL40B2 beamline in SPring-8 and at the BL-6A beamline (Shimizu et al., 2013) in KEK-PF. A quartz capillary cell with the diameter of 2.0 mmϕ was fixed in an aluminum block. The same capillary cell was used for the solution, solvent, and the reference solution, that is, a standard PEO sample **SE-5** (Tosoh, Japan) with the M_w and $Đ$ being 37.6 or 44.2 kg mol^{-1} and 1.03 or 1.17 both depending on the lot number, respectively. The wavelength λ_0 was chosen as 0.10 and 0.15 nm

for SPring-8 and KEK-PF, respectively. The camera length, that is, the distance from the sample to the detector, was 4.2 m and 2.6 m for the two beamlines. Dectris PILATUS3 2M and PILATUS 1M detectors were used to determine the scattering intensity as a function of the magnitude q of the scattering vector with a SAngler circular averaging software (Shimizu et al., 2016). Silver behenate was used to determine the q value of each pixel on the detectors. The temperature was controlled by a Peltier element. The excess scattering intensity $\Delta I(q)$ was evaluated by the numerical difference of scattering intensities between the solution and the solvent; note that each scattering intensity was calibrated by the intensity of the direct beam detected at the lower end of the solution cell to compensate both the intensity fluctuation of the incident light and the transparency of the solution. The ratio R_q/K of the Rayleigh ratio R_q to the optical constant K was estimated from the following equation (Glatter & Kratky, 1982; Ishida, Yoshida, & Terao, 2019)

$$\frac{R_q}{K} = M_{\mathrm{w,PEO}} \left(\frac{\Delta z_{\mathrm{PEO}}}{\Delta z}\right)^2 \left[\frac{c_{\mathrm{PEO}}}{\Delta I_{\mathrm{PEO}}(q)}\right]_{c\to 0, q\to 0} \Delta I(q) \quad (1)$$

where the subscript PEO denotes the value for the standard PEO sample and Δz is defined as

$$\Delta z = z - v_{\mathrm{p}}\rho_{\mathrm{e,s}} \quad (2)$$

Here, z, v_{p}, and $\rho_{\mathrm{e,s}}$ are the number of moles of electron per unit mass of the solute, the partial specific volume, and the electron density of the solvent, respectively. These values were calculated from the density of the solution and the solvent.

2.4. Viscometry

The specific viscosity η_{sp} in the renatured process for **X341k** in 10 mM aqueous NaCl was measured at 20 °C with a Ubbelohde type viscometer. Just after the solution with c = 6 mg mL^{-1} was treated at 80 °C for 1 h and abruptly cooled to 17 °C, it was diluted to c = 1 mg mL^{-1}. Then, the solution was poured into the viscometer thermostated at 20 °C.

3. Results & discussion

3.1. Molar mass of as-prepared and renatured xanthan samples

The obtained SEC-MALS data, the retention volume V_{e} dependence of c and M_{w}, are shown in Fig. 2. The averaged M_{w} and $Đ$ values calculated from the data for each sample are summarized in Table 1. The evaluated M_{w} values for the as-prepared samples were consistent with those from the universal calibration method within the experimental error (± 5%) while the $Đ$ values are larger, that is 1.6, 1.6, and 1.8 for **X341k**, **X400k**, and **X461k**, respectively. This is probably because of insufficient resolution of the current column set for our xanthan samples to evaluate M_{n} accurately, suggesting the actual $Đ$ values may be between those from the two methods. The resulting M_{w} values for **X341k** at C_{s} = 5 mM are smaller than that in 100 mM aqueous NaCl, indicating partly unfolded structure in the low ionic strength solvent. The molar mass values of the renatured samples are substantially the same as or somewhat larger than the as-prepared sample except for **X341k** at C_{s} = 5 mM, suggesting the existence of double helical aggregates composed of more than two xanthan molecules as is found in the previous research (Matsuda et al., 2009). Indeed, the gyration radii R_{g} data for some renatured samples were appreciably smaller than that for the native samples with the same M_{w} as illustrated in Fig. S1. Somewhat larger η_{sp}/c value for the renatured solution as shown in Fig. S2 supports this suggestion. This figure also shows that almost no time dependence of η_{sp}/c was observed in the range of t < 1000 s after the cooling.

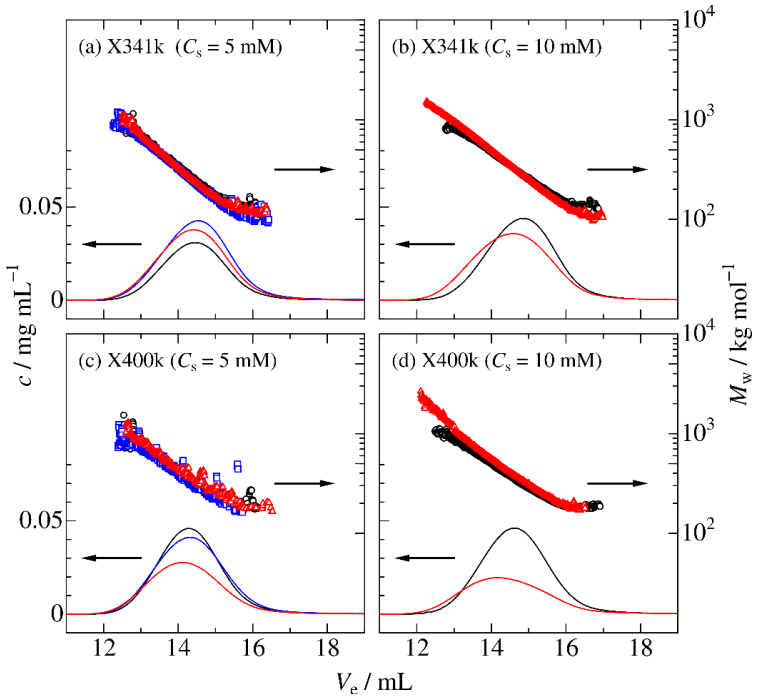

Fig. 2. Retention volume V_e dependence of the polymer mass concentration c (curves) and the weight-average molar mass M_w (symbols) for (a) **X341k** at C_s = 5 mM, (b) **X341k** at C_s = 10 mM, (c) **X400k** at C_s = 5 mM, and (d) **X400k** at C_s = 10 mM. Black, blue, and red symbols (or curves) denote the data for the as-prepared solution, the renatured solution at c_d between 3.0 and 3.1 mg mL^{-1}, and the renatured solution at c_d between 5.4 and 6.4 mg mL^{-1}, respectively.

Table 1
Molar masses of xanthan samples

Sample	c_d / mg mL^{-1}	C_s / mM	M_w / kg mol^{-1}	$Đ$
X341k	As Prepared	100	341	1.3 (1.6 ***a***)
	As Prepared	10	331	1.2
	6.1	10	413	1.4
	As Prepared	5	298	1.2
	3.1	5	285	1.3
	6.4	5	322	1.4
X400k	As Prepared	100	400	1.2 (1.6 ***a***)
	As Prepared	10	390	1.2
	5.4	10	573	1.4
	As Prepared	5	384	1.2
	3.0	5	404	1.2
	6.2	5	534	1.3
X461k	As Prepared	100	461	1.1 (1.8 ***a***)

***a*:** From universal calibration.

3.2. Circular dichroism spectra including vacuum ultraviolet region

CD spectra for the xanthan samples in 10 mM aqueous NaCl are illustrated in Fig. 3, in which the data obtained from the two apparatuses are substantially the same for the overlapped λ_0 range between 210 and 250 nm. It was difficult to acquire the data below λ_0 = 180 nm even by using the synchrotron radiation owing to the absorption of NaCl. The specific ellipticity $[\theta']$ for the disordered xanthan at 80 °C in the range between λ_0 = 187 and 218 nm are appreciably smaller than those for the ordered xanthan at 20 °C. This λ_0 range is suitable to observe the conformational change of xanthan because of smaller difference in the vacuum ultraviolet region below λ_0 = 187 nm. Essentially the same CD spectra were found at 20 °C both before and two days after the heating, indicating that local optically active structure of renatured xanthan is substantially the same as that for the as-prepared solution.

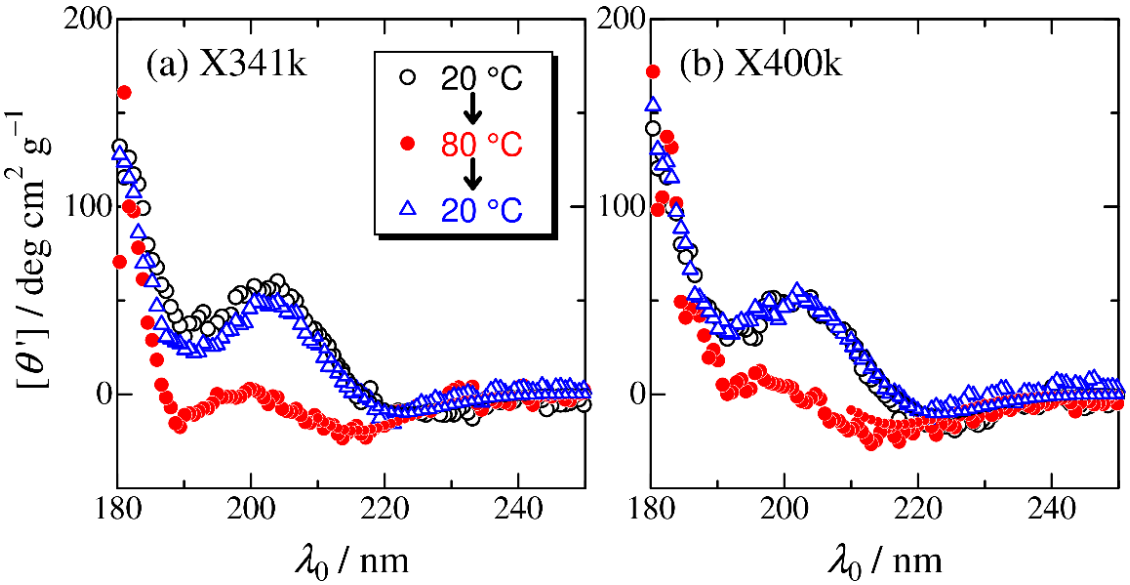

Fig. 3. CD spectra for (a) **X341k** and (b) **X400k** in 10 mM aqueous NaCl. Polymer mass concentration was adjusted around 6 mg mL^{-1}. Black unfilled circles, red filled circles, and blue triangles indicate the data for native sample at 20 °C, denatured sample at 80 °C, and renatured sample (at 20 °C) incubated for 2 days after cooled from 80 °C. Large and small symbols, data from HiSOR and the lab equipment, respectively.

3.3. Temperature-induced conformational change detected by CD

The temperature of order-disorder conformational change was estimated by the CD measurement with raising temperature as illustrated in Fig. S3 for **X341k** and **X461k** in aqueous NaCl. The specific ellipticity $[\theta']_{210}$ at λ_0 = 210 nm and at C_s = 10 mM decreases rapidly between 50 and 65 °C both for the samples, indicating that the current xanthan samples have the completely ordered structure at 20 °C and the mostly disordered conformation at 80 °C. Lower conformational change temperature between 45 and 60 °C was observed in 5 mM aqueous NaCl.

3.4. Time course of CD after rapid heating or cooling

Time-resolved data of $[\theta']_{210}$ after the rapid heating from 20 °C to 80 °C are displayed in Fig. 4 for the three xanthan samples along with those for the rapid cooling from 80 °C to 20 °C. The time zero is defined as the time when the cell was installed in the thermostatic cell holder and the temperature of the inside solution became substantially the same temperature (< ±1 °C) as the

target temperature at most 150 s; noted that it was less than 30 s to pass through the conformational change temperature. The $[\theta']_{210}$ value for the rapid heating reaches the completely denatured value (red line) at most 200 s, indicating that the denature process observed by $[\theta']_{210}$ is faster than or comparable to the heating rate.

On the other hand, gradual increase of $[\theta']_{210}$ was observed for the rapid cooling process. The $[\theta']_{210}$ data at 1800 s are still smaller than that for the ordered structure while they mostly reach the blue line for the as-prepared solution after 80,000 s (22 h) and 160,000 s (44 h) later, clearly indicating that the renature process observed by $[\theta']_{210}$ is much slower than the cooling rate. Slightly smaller $[\theta']_{210}$ at the longest t than the as-prepared sample can be attributed to the branching conformation (Matsuda et al., 2009) at which the xanthan chains cannot form the double helical structure properly. Similar tendency was also observed at λ_0 = 200 nm for **X341k** and **X400k** in 10 mM aqueous NaCl (Fig. S4). The first-order plot, that is, $\ln[\{[\theta']_{210}(\infty) - [\theta']_{210}(t)\}/\{[\theta']_{210}(\infty) - [\theta']_{210}(0)\}]$ vs t, assuming that $[\theta']_{210}(t)$ at t = 44 h is referred to as $[\theta']_{210}(\infty)$, is shown in Fig. S5. The data points follow a straight line while the intercepts at $t = 0$ are appreciably smaller than zero, suggesting that the conformational change is faster at higher temperature, or a certain faster process exists in the disorder-order conformational change. We estimated the first-order rate constant k of this slow process to be 6×10^{-5} s^{-1} and 4×10^{-5} s^{-1} for **X341k** and **X400k**, respectively.

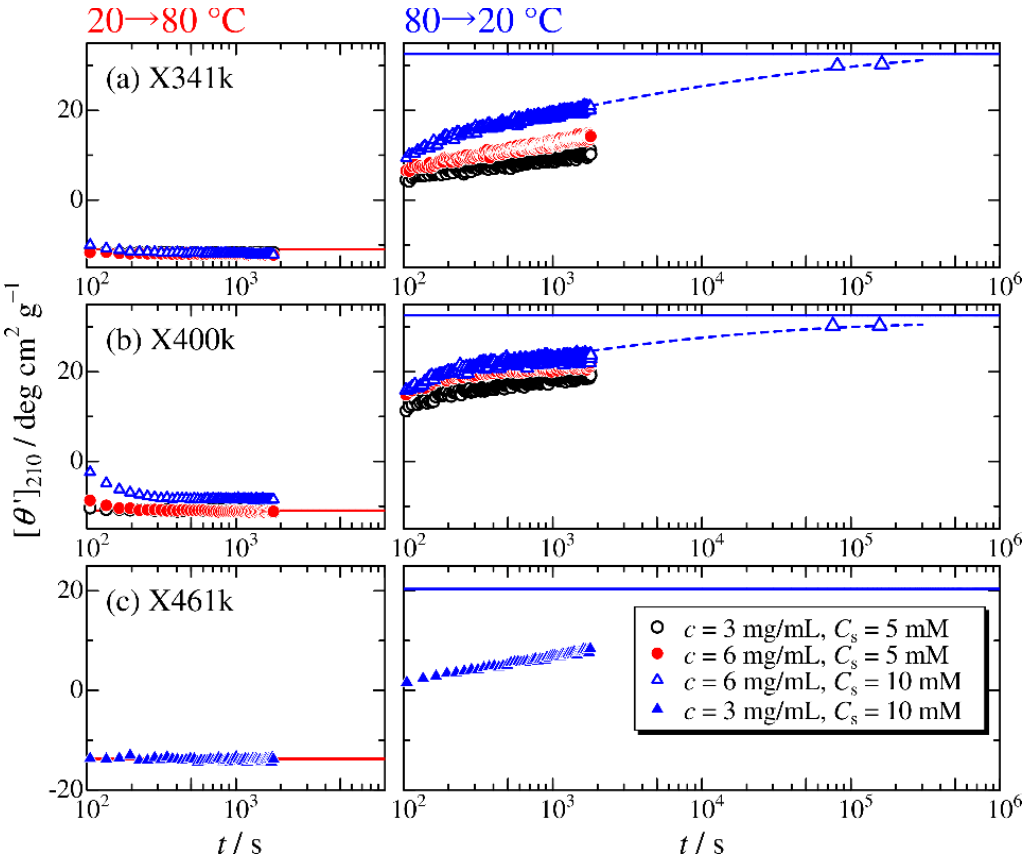

Fig. 4. Time course of $[\theta']_{210}$ for (a) **X341k**, (b) **X400k**, and (c) **X461k** in aqueous NaCl. Left, abruptly heated from 20 to 80 °C. Right, abruptly cooled from 80 to 20 °C. Black unfilled circles, red filled circles, blue unfilled triangles, and blue filled triangles denote C_s = 5 mM and c = 3 mg

mL^{-1}, C_s = 5 mM and c = 6 mg mL^{-1}, C_s = 10 mM and c = 6 mg mL^{-1}, and C_s = 10 mM and c = 3 mg mL^{-1}, respectively. Solid blue lines, the $[\theta']_{210}$ value for the as-prepared solution at 20 °C.

3.5. Time-dependent scattering intensities for xanthan solutions

The reduced scattering intensity R_q/Kc is plotted against the magnitude q of the scattering vector in Fig. 5, in which doubly extrapolated value to c = 0 and q = 0 is the weight-average molar mass M_w of the solute. Taking into consideration that the qR_q/Kc value for the thin rod approaches the asymptotic value (W Burchard, 1994; Holtzer, 1955) of πM_L with M_L being the molar mass per unit contour length, R_q/Kc at the middle q region mainly reflects the M_L value which is the key factor to determine the single or double stranded structures; it is noted that the chain thickness may affect the R_q/Kc data at high q region and the structure factor $S(q)$, the chain stiffness (L_k), and $Đ$ influence the R_q/Kc only in the low q region. Indeed, we accurately determined the M_L value for semiflexible polysaccharides including amylose, cellulose (Jiang, Kitamura, Sato, & Terao, 2017) and single stranded schizophyllan (Tomofuji, Yoshiba, Christensen, & Terao, 2019) from the SAXS intensity in the middle q range.

Fig. 5 indicates the scattering data for xanthan samples in solution at 80 °C at different t after the capillary cell was installed into the thermostatic cell holder. It takes similar time to attain the target temperature to that for our CD equipment (< 150 s). It should be noted that the data at t = 0 were measured at 20 °C without heat treatment. In contrast to the above-mentioned CD data, appreciable time dependent scattering intensity was observed after t = 150 s, clearly indicating that the time course of the main-chain conformation observed by SAXS is different from the side-chain conformation from CD.

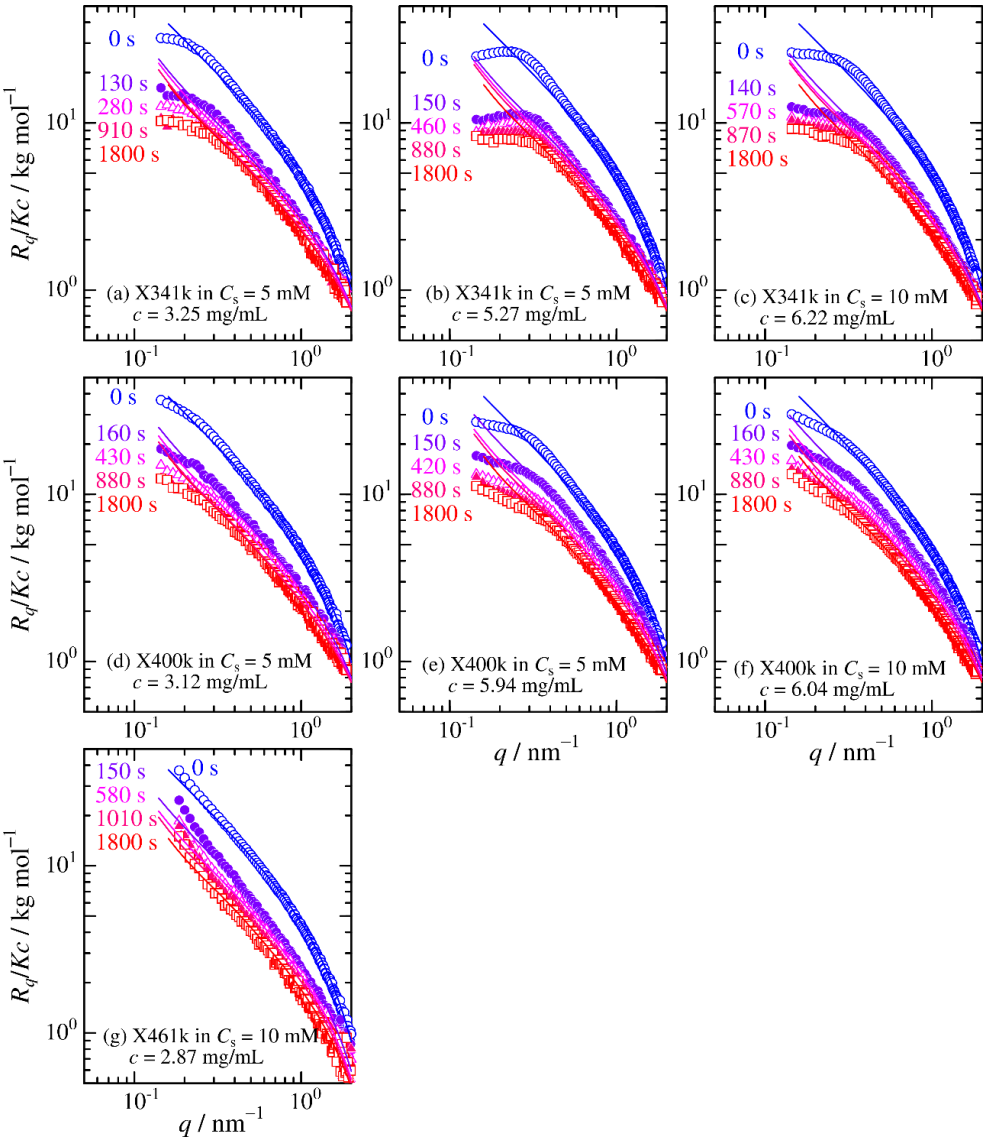

Fig. 5. Double logarithmic plots of R_q/Kc vs q for indicated samples and concentrations after abrupt heat treatment from 20 °C to 80 °C. Blue circles, data for native xanthan at 20 °C, referred to as t = 0 s. The other data are those after abruptly heat to 80 ° C. Blue and red curves for t = 0 s and 1800 s are calculated in terms of the wormlike chain model with the parameters in Table 2. Other curves are the theoretical values calculated from eq 6 with α in Fig. 7.

SAXS profiles for the rapid cooling process from 80 °C to 20 °C are shown in Fig. 6. The scattering intensities after cooling are quite larger than that at t = 0 which was observed at 80 °C after the solution was kept at 80 °C at least 30 min. Interestingly, substantially the same scattering profiles were observed between 150 s and 1800 s, indicating that the conformational change from the disordered to ordered states is essentially faster than the other processes. This is completely opposite tendency comparing with those from CD.

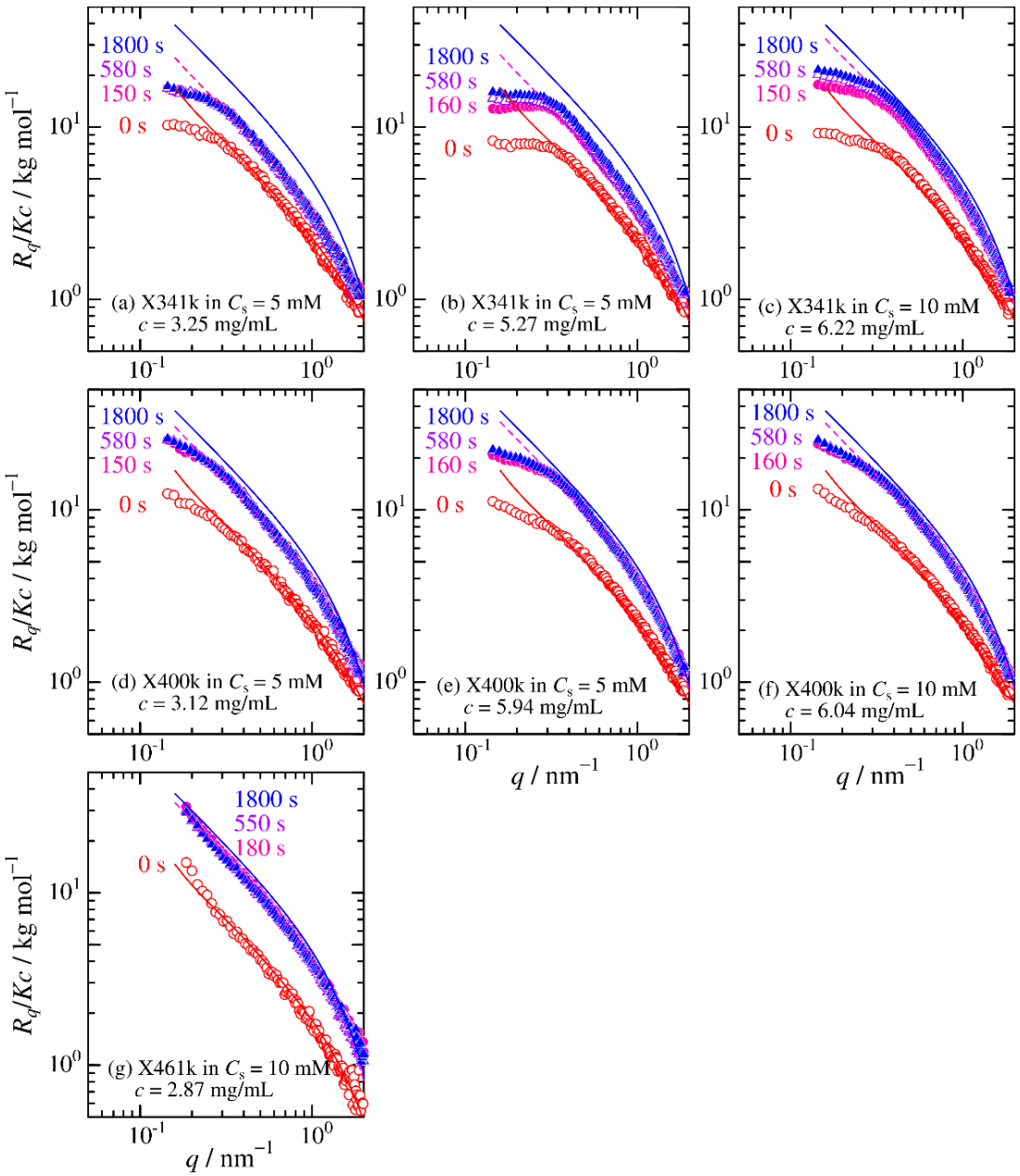

Fig. 6. Double logarithmic plots of R_q/Kc vs q for indicated samples and concentrations after abrupt cool treatment from 80 °C to 20 °C. Red circles, data for completely denatured xanthan at 80 °C, referred to as t = 0 s. The other data are the data after abruptly heat to 80 °C. Red and blue curves are the same as that in Fig. 5. Dashed curves are the theoretical values calculated from eq 6 with α in Fig. 7.

3.6. Analysis in terms of the wormlike chain

To analyze the above-mentioned SAXS data, we utilized the touched-bead wormlike chain model. The reduced scattering intensity R_q/Kc can be written as (W. Burchard & Kajiwara, 1970; Yamakawa & Yoshizaki, 2016)

$$\frac{R_q}{Kc} = M_w P(q) S(q) \quad (3)$$

where

$$P(q) = 9\left(\frac{2}{qd}\right)^6 \left(\sin\frac{qd}{2} - \frac{qd}{2}\cos\frac{qd}{2}\right)^2 P_{\text{thin}}(q) \quad (4)$$

Here, d is the bead diameter and $P_{\text{thin}}(q)$ is the form factor of the thin wormlike chain, which is calculated with the characteristic function $I(qL_k ; u/L_k)$ by

$$P_{\text{thin}}(q) = \frac{2}{L^2}\int_0^L (L-u) I(qL_k; u/L_k)\mathrm{d}u \quad (5)$$

with L and L_k being the contour length and the Kuhn segment length (a measure of the chain stiffness), respectively. The integral was numerically calculated with the Nakamura-Norisuye expression (Nakamura & Norisuye, 2004, 2008) of $I(qL_k ; u/L_k)$. Since $qP_{\text{thin}}(q)$ reaches an asymptotic value of π/L_w with L_w being weight-average contour length at high q limit (Holtzer, 1955; Yamakawa & Yoshizaki, 2016) and $S(q)$ can be regarded as unity except for the low-q region, $qR_q/Kc = qS(q)P_{\text{thin}}(q)M_w$ for the thin wormlike chain reaches πM_L; note that $M_L = M_w/L_w$. Assuming previously estimated chain stiffness both for the ordered (Sato, Norisuye, et al., 1984a) and the disordered (Liu et al., 1987) conformations, that is, L_k = 240 and 42 nm, respectively, and M_w values determined by SEC-MALS, the other two parameters, M_L and d, are unequivocally determined for equilibrium data designated as 0 s both in Figs. 5 and 6 by means of the curve fitting procedure (see also Figs S6 and S7 for the enlarged view of the middle q range). Substantially no concentration dependence was obtained for the two parameters, M_L and d, suggesting the assumption of $S(q) = 1$ is reasonable. The evaluated M_L values for the ordered and disordered structures are consistent with the literature values (Matsuda et al., 2009). The parameters are summarized in Table 2. The theoretical values reproduce the experimental data at 0 s in Figs. 5 and 6 except for the low q region ($q < 0.3$ nm^{-1}) where $S(q)$ may not be ignorable there because of the repulsive interactions between xanthan chains. Somewhat smaller R_q/Kc in the cooling process (Fig. 6) at finite t is likely because of the partly unfolded conformation. The discrepancy is more significant for **X341k** in 5 mM aqueous NaCl. This is reasonable because the lower M_w value in the solvent than those for the as-prepared solutions as shown in Table 1. We note that substantially the same theoretical curves will be obtained even if we assumed the half molar mass for the disordered state or quasi star-like conformation with short rod region at 80 °C reported previously (Liu et al., 1987) because the chain architecture affects the scattering intensity only in the low-q region; the form factor of the wormlike star chain can be calculated by the Huber and Burchard expression (Huber & Burchard, 1989) as described in our recent report for semiflexible star polymers (Hasegawa, Nagata, Terao, & Suginome, 2017).

Table 2.
Wormlike chain parameters of the xanthan samples

Sample	State	M_w / kg mol^{-1}	L_K / nm	M_L / kg mol^{-1} nm^{-1}	d / nm
X341k	ordered ***b***	341 ***a***	240 ***a***	2.02 ± 0.12	2.3 ± 0.1
	disordered ***c***	341 ***a***	42 ***a***	0.81 ± 0.17	1.6 ± 0.1
X400k	ordered ***b***	400 ***a***	240 ***a***	1.99 ± 0.05	2.3 ± 0.1
	disordered ***c***	400 ***a***	42 ***a***	0.81 ± 0.03	1.6 ± 0.1
X461k	ordered ***b***	461 ***a***	240 ***a***	1.93 ± 0.08	2.4 ± 0.2
	disordered ***c***	461 ***a***	42 ***a***	0.70 ± 0.02	2.1 ± 0.2

a**:** Assumed, ***b*****:** For as-prepared samples at 20 °C, ***c*****:** kept at 80 °C for t = 1800 s.

As mentioned above, scattering data in the heating process below t = 1000 s reflects the mixture of the ordered and disordered conformations. When we assume the two-state model in which completely ordered (O) and disordered (D) chains, R_q/Kc can be written as

$$\frac{R_q}{Kc} = S(q)\left[\alpha M_{w,O} P_O(q) + (1-\alpha) M_{w,D} P_D(q)\right] \quad (6)$$

where α is the degree of dissociation and subscripts O and D denote the ordered and disordered states. Further assuming $S(q)$ = 1 and that the parameters for the ordered and disordered conformations are the same as those in Table 2 at 20 and 80 °C, respectively, the theoretical R_q/Kc values with an adjustable parameter α fit the experimental data in substantially the same q range described above. The obtained α values are plotted against t in Fig. 7. In the heating process, α gradually decreases with increasing t. This may be regarded as the first order process taking into consideration that this is the unfolding process of the double helix. Indeed, the plots of ln α vs t (see Fig. S8) follow a straight line. Upward deviation in the initial time range implies a certain faster process for the order-disorder conformation change. The first-order reaction rate k estimated from the straight line in Fig. S8 ranges between 1×10^{-3} and 2×10^{-3} s^{-1} for all the samples. On the contrary, no time dependence was observed for the cooling process, indicating that double stranded conformation is recovered quickly. The α values are however smaller than unity for the renatured samples. This is most likely because the complete double helical conformation cannot be formed by the hairpin like conformation or the branching aggregates as in the case of the CD data or partly unfolded conformation due to low ionic strength.

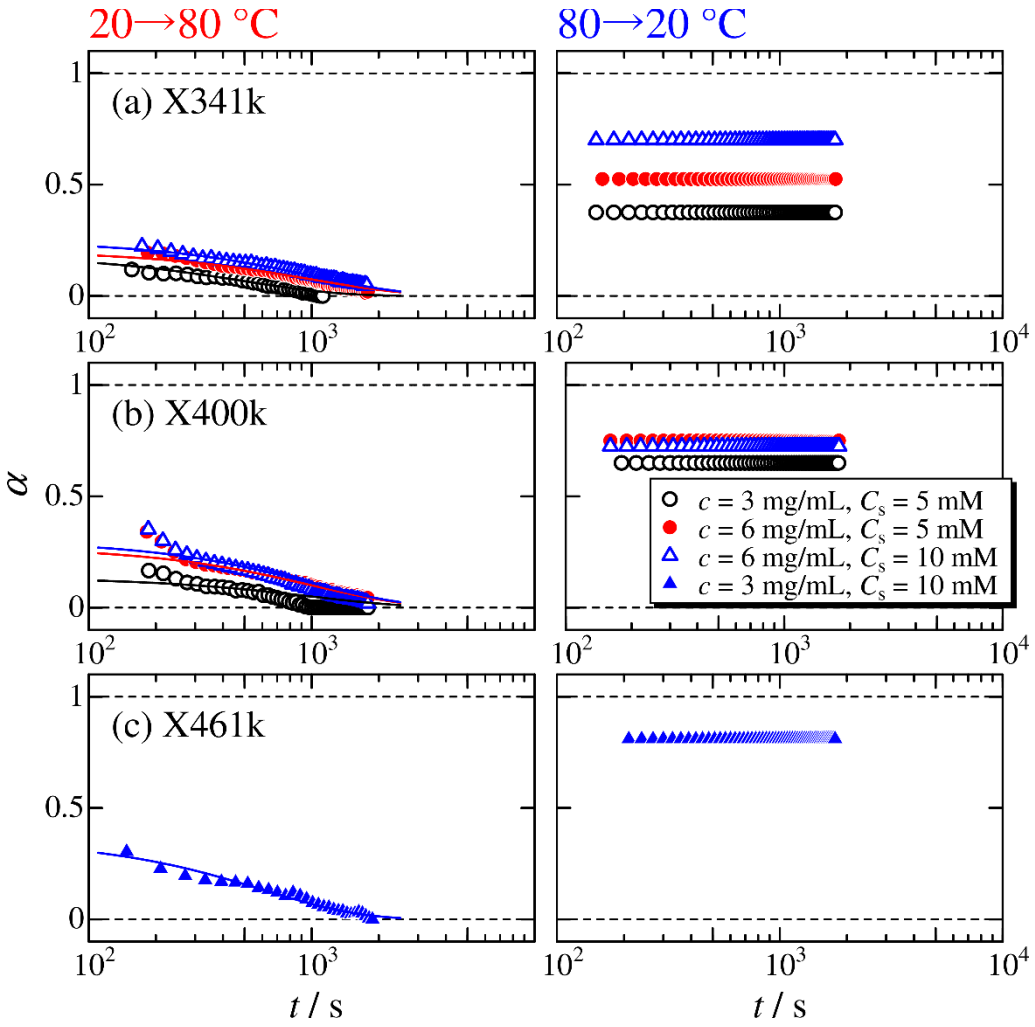

Fig. 8. Time course of α for (a) **X341k**, (b) **X400k**, and (c) **X461k** in aqueous NaCl. Left, abruptly heated from 20 to 80 °C. Right, abruptly cooled from 80 to 20 °C. Black unfilled circles, red filled circles, blue unfilled triangles, and blue filled triangles denote C_s = 5 mM and c = 3 mg mL^{-1}, C_s = 5 mM and c = 5 – 6 mg mL^{-1}, C_s = 10 mM and c = 6 mg mL^{-1}, and C_s = 10 mM and c = 3 mg mL^{-1}, respectively. Solid curves indicate the first order reaction with the same rate constant shown in Fig. S8.

3.7. *Kinetics of thermal conformational change*

The current analysis of the time-resolved CD and SAXS measurements clearly showed that both denature and renature processes consist of at least two steps, and hence the existence of some intermediate species as illustrated in Fig. 8. If we consider the CD signals mainly reflect the chiral order of the carbonyl groups on the side chains of xanthan c.f. Fig. 1, the initial change after the rapid heating is mainly the melting of the side chain conformation while the double helical structure remains. This can be regarded as loose double helix. It takes 30 min to attain the complete disordered state with the first-order reaction rate of 1 – 2 $\times 10^{-3}$ s^{-1}. On the other hand, formation of the double helical structure is faster than the temperature changing (< 150 s) after rapid cooling. This double helix may be somewhat looser than the native state because the CD signal was still changing at t = 150 s. The reaction to attain the native double helix obey the first

order rate constant of $4 - 6 \times 10^{-5}$ s^{-1}, then more than 1 day was needed to recover similar CD signal as that for the as-prepared solution. According to the previous reports (Morris, 2019; Norton et al., 1984), the molar mass of xanthan recorded by light scattering with raising temperature decreased at lower temperature than those for the reduction of helix content estimated from optical rotation, suggesting a single helix conformation as an intermediate state. On the one hand, in the case of rapid temperature change of the current study, we found that the quick formation of the (loose) double helical structure, which may also be important to understand the temperature and solvent dependent conformation and aggregation of xanthan.

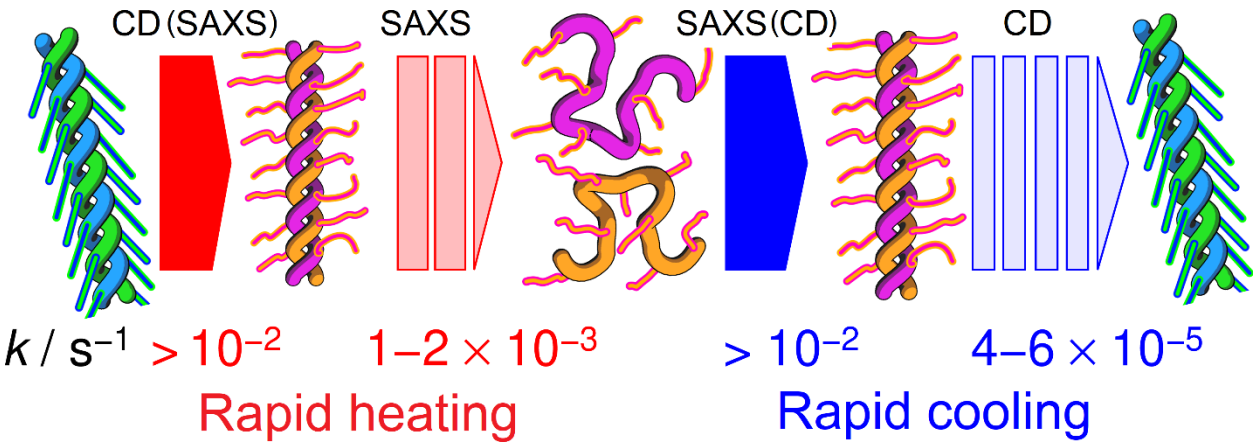

Fig. 8. Schematic representation of denaturation and renaturation processes of xanthan in aqueous NaCl.

4. Conclusions

Time-resolved measurement of CD and SAXS were made for the three xanthan samples ranging in M_w between 300 and 500 kg mol^{-1} in aqueous NaCl at C_s = 5 mM and 10 mM. Appreciably different kinetics was found between the ellipticity and the scattering profile in the middle q region, clearly indicating the intermediate species, loose double stranded conformation, in which the side chain is still disordered. This loose double helix was found both after the rapid heating and cooling processes. The current finding may be applicable for the higher M_w xanthan samples whereas the SAXS measurement becomes more difficult owing to higher melting temperature in aqueous NaCl solutions. The variety of higher order structure of xanthan reported in the literatures (Capron et al., 1997; Matsuda et al., 2009) may be related to the kinetics. In other words, not only static properties including temperature, concentration, chain length, but also kinetic properties such as temperature changing rate may play an important role for the higher order structure and rheological properties of renatured xanthan. The current method can be applied for the other multiple helical polysaccharides (Meng, Lyu, Xu, & Zhang, 2020) to clarify the kinetic behavior to form the higher order structures.

Declaration of Competing Interest

The authors reported no declarations of interest.

Acknowledgement

The authors are grateful to Prof. Takahiro Sato (Osaka Univ.) for fruitful discussion and to Prof. Nobutaka Shimizu (KEK), Prof. Noriyuki Igarashi (KEK), and Dr. Noboru Ohta (SPring-8) for SAXS measurements. The synchrotron radiation experiments were performed at the BL-6A beamline in KEK-PF (Proposal Nos. 2017G023 and 2018G519) and at the BL40B2 in SPring-8

with the approval of the Japan Synchrotron Radiation Research Institute (JASRI) (Proposal Nos. 2017B1062, 2018B1088, 2019A1072, and 2019B1113). CD spectroscopy was carried out with the approval of the Hiroshima Synchrotron Radiation Center (HiSOR) of Hiroshima University (Proposal No. 19BU011). This work was partly supported by JSPS KAKENHI Grant Numbers JP17K05884, JP18H02020, and JP20H02788.

Appendix A. Supplementary data

Supplementary material related to this article can be found in the online version, at doi:

References

Bercea, M., & Morariu, S. (2020). Real-time monitoring the order-disorder conformational transition of xanthan gum. *Journal of Molecular Liquids,* 309, 113168.

Brunchi, C. E., Avadanei, M., Bercea, M., & Morariu, S. (2019). Chain conformation of xanthan in solution as influenced by temperature and salt addition. *Journal of Molecular Liquids,* 287, 111008.

Burchard, W. (1994). *Light Scattering Techniques*. In S. B. Ross-Murphy (Ed.), *Physical Techniques for the Study of Food Biopolymers* (pp. 151-213). Boston, MA: Springer US

Burchard, W., & Kajiwara, K. (1970). The statistics of stiff chain molecules. I. The particle scattering factor. *Proceedings of the Royal Society A: Mathematical, Physical and Engineering Sciences,* 316(1525), 185-199.

Camesano, T. A., & Wilkinson, K. J. (2001). Single Molecule Study of Xanthan Conformation Using Atomic Force Microscopy. *Biomacromolecules,* 2(4), 1184-1191.

Capron, I., Alexandre, S., & Muller, G. (1998). An atomic force microscopy study of the molecular organisation of xanthan. *Polymer,* 39(23), 5725-5730.

Capron, I., Brigand, G., & Muller, G. (1997). About the native and renatured conformation of xanthan exopolysaccharide. *Polymer,* 38(21), 5289-5295.

Choppe, E., Puaud, F., Nicolai, T., & Benyahia, L. (2010). Rheology of xanthan solutions as a function of temperature, concentration and ionic strength. *Carbohydrate Polymers,* 82(4), 1228-1235.

Dalheim, M. Ø., Christensen, B. E., Comesse, S., & Renou, F. (2020). *Modification of xanthan in the ordered and disordered states*. In A. P. Rauter, B. E. Christensen, L. Somsák, P. Kosma & R. Adamo (Eds.), *Recent Trends in Carbohydrate Chemistry* (pp. 403-440): Elsevier

Glatter, O., & Kratky, O. (1982). *Small Angle X-ray Scattering*. London: Academic Press.

Grubisic, Z., Rempp, P., & Benoit, H. (1967). A Universal Calibration for Gel Permeation Chromatography. *Journal of Polymer Science Part B-Polymer Letters,* 5(9pb), 753-&.

Hasegawa, H., Nagata, Y., Terao, K., & Suginome, M. (2017). Synthesis and Solution Properties of a Rigid Helical Star Polymer: Three-Arm Star Poly(quinoxaline-2,3-diyl). *Macromolecules,* 50(19), 7491-7497.

Holtzer, A. (1955). Interpretation of the Angular Distribution of the Light Scattered by a Polydisperse System of Rods. *Journal of Polymer Science,* 17(85), 432-434.

Huber, K., & Burchard, W. (1989). Scattering Behavior of Wormlike Star Macromolecules. *Macromolecules,* 22(8), 3332-3336.

Hublik, G. (2012). *Xanthan*. In K. Matyjaszewski & M. Möller (Eds.), *Polymer Science: A Comprehensive Reference* (pp. 221-229). Amsterdam: Elsevier

Ikeda, S., Gohtani, S., Nishinari, K., & Zhong, Q. X. (2012). Single Molecules and Networks of Xanthan Gum Probed by Atomic Force Microscopy. *Food Science and Technology Research,* 18(5), 741-745.

Ishida, S., Yoshida, T., & Terao, K. (2019). Complex formation of a triple-helical peptide with sodium heparin. *Polymer Journal,* 51(11), 1181-1187.

Jiang, X. Y., Kitamura, S., Sato, T., & Terao, K. (2017). Chain Dimensions and Stiffness of Cellulosic and Amylosic Chains in an Ionic Liquid: Cellulose, Amylose, and an Amylose Carbamate in BmimCl. *Macromolecules,* 50(10), 3980-3985.

Kawaguchi, S., Imai, G., Suzuki, J., Miyahara, A., & Kitano, T. (1997). Aqueous solution properties of oligo- and poly(ethylene oxide) by static light scattering and intrinsic viscosity. *Polymer,* 38(12), 2885-2891.

Kitamura, S., Takeo, K., Kuge, T., & Stokke, B. T. (1991). Thermally induced conformational transition of double-stranded xanthan in aqueous salt solutions. *Biopolymers,* 31(11), 1243-1255.

Kool, M. M., Gruppen, H., Sworn, G., & Schols, H. A. (2013). Comparison of xanthans by the relative abundance of its six constituent repeating units. *Carbohydrate Polymers,* 98(1), 914-921.

Kratky, O., & Porod, G. (1949). Rontgenuntersuchung Geloster Fadenmolekule. *Recueil Des Travaux Chimiques Des Pays-Bas-Journal of the Royal Netherlands Chemical Society,* 68(12), 1106-1122.

Kumar, A., Rao, K. M., & Han, S. S. (2018). Application of xanthan gum as polysaccharide in tissue engineering: A review. *Carbohydrate Polymers,* 180, 128-144.

Liu, W., & Norisuye, T. (1988a). Order-Disorder Conformation Change of Xanthan in 0.01m Aqueous Sodium-Chloride - Dimensional Behavior. *Biopolymers,* 27(10), 1641-1654.

Liu, W., & Norisuye, T. (1988b). Thermally Induced Conformation Change of Xanthan - Interpretation of Viscosity Behavior in 0.01-M Aqueous Sodium-Chloride. *International Journal of Biological Macromolecules,* 10(1), 44-50.

Liu, W., Sato, T., Norisuye, T., & Fujita, H. (1987). Thermally Induced Conformational Change of Xanthan in 0.01m Aqueous Sodium-Chloride. *Carbohydrate Research,* 160, 267-281.

Matsuda, Y., Biyajima, Y., & Sato, T. (2009). Thermal Denaturation, Renaturation, and Aggregation of a Double-Helical Polysaccharide Xanthan in Aqueous Solution. *Polymer Journal,* 41(7), 526-532.

Matsuda, Y., Okumura, K., & Tasaka, S. (2018). Molar mass dependence of structure of xanthan thermally denatured and renatured in dilute solution. *Polymer Journal,* 50(11), 1043-1049.

Matsuda, Y., Sugiura, F., Mays, J. W., & Tasaka, S. (2015). Atomic force microscopy of thermally renatured xanthan with low molar mass. *Polymer Journal,* 47(3), 282-285.

Matsuda, Y., Sugiura, F., Okumura, K., & Tasaka, S. (2016). Renaturation behavior of xanthan with high molar mass and wide molar mass distribution. *Polymer Journal,* 48(5), 653-658.

Matsuo, K., & Gekko, K. (2013). Construction of a Synchrotron-Radiation Vacuum-Ultraviolet Circular-Dichroism Spectrophotometer and Its Application to the Structural Analysis of Biomolecules. *Bulletin of the Chemical Society of Japan,* 86(6), 675-689.

Matsuo, K., Sakai, K., Matsushima, Y., Fukuyama, T., & Gekko, K. (2003). Optical Cell with a Temperature-Control Unit for a Vacuum-Ultraviolet Circular Dichroism Spectrophotometer. *Analytical Sciences,* 19(1), 129-132.

Meng, Y., Lyu, F., Xu, X., & Zhang, L. (2020). Recent Advances in Chain Conformation and Bioactivities of Triple-Helix Polysaccharides. *Biomacromolecules,* 21(5), 1653-1677.

Merino-González, A., & Kozina, A. (2017). Influence of aggregation on characterization of dilute xanthan solutions. *International Journal of Biological Macromolecules,* 105, 834-842.
Moffat, J., Morris, V. J., Al-Assaf, S., & Gunning, A. P. (2016). Visualisation of xanthan conformation by atomic force microscopy. *Carbohydrate Polymers,* 148, 380-389.
Morris, E. R. (2019). Ordered conformation of xanthan in solutions and "weak gels": Single helix, double helix – or both? *Food Hydrocolloids,* 86, 18-25.
Nakamura, Y., & Norisuye, T. (2004). Scattering function for wormlike chains with finite thickness. *Journal of Polymer Science Part B-Polymer Physics,* 42(8), 1398-1407.
Nakamura, Y., & Norisuye, T. (2008). *Brush-like polymers*. In R. Borsali & R. Pecora (Eds.), *Soft Matter Characterization* (pp. 235-286): Springer Netherlands
Nishinari, K., Turcanu, M., Nakauma, M., & Fang, Y. (2019). Role of fluid cohesiveness in safe swallowing. *NPJ Sci Food,* 3(1), 5.
Norton, I. T., Goodall, D. M., Frangou, S. A., Morris, E. R., & Rees, D. A. (1984). Mechanism and dynamics of conformational ordering in xanthan polysaccharide. *Journal of Molecular Biology,* 175(3), 371-394.
Norton, I. T., Goodall, D. M., Morris, E. R., & Rees, D. A. (1980). Kinetic Evidence for Intramolecular Conformational Ordering of the Extracellular Polysaccharide (Xanthan) from Xanthomonas-Campestris. *Journal of the Chemical Society, Chemical Communications*(12), 545-547.
Okuyama, K., Arnott, S., Moorhouse, R., Walkinshaw, M. D., Atkins, E. D. T., & Wolf-Ullish, C. H. (1980). *Fiber Diffraction Studies of Bacterial Polysaccharides*. In *Fiber Diffraction Methods* (pp. 411-427): American Chemical Society
Otsubo, M., & Terao, K. (2021). Kinetics of the complex formation of silica nanoparticles with collagen. *Polymer Journal*, in press. DOI:10.1038/s41428-021-00553-4.
Oviatt, H. W., & Brant, D. A. (1994). Viscoelastic Behavior of Thermally Treated Aqueous Xanthan Solutions in the Semidilute Concentration Regime. *Macromolecules,* 27(9), 2402-2408.
Papagiannopoulos, A., Sotiropoulos, K., & Pispas, S. (2016). Particle tracking microrheology of the power-law viscoelasticity of xanthan solutions. *Food Hydrocolloids,* 61, 201-210.
Papagiannopoulos, A., Sotiropoulos, K., & Radulescu, A. (2016). Scattering investigation of multiscale organization in aqueous solutions of native xanthan. *Carbohydrate Polymers,* 153, 196-202.
Pasch, H. (2012). *2.03 - Chromatography A2 - Matyjaszewski, Krzysztof*. In M. Möller (Ed.), *Polymer Science: A Comprehensive Reference* (pp. 33-64). Amsterdam: Elsevier
Rinaudo, M. (2008). Main properties and current applications of some polysaccharides as biomaterials. *Polymer International,* 57(3), 397-430.
Sato, T., Kojima, S., Norisuye, T., & Fujita, H. (1984). Double-Stranded Helix of Xanthan in Dilute-Solution - Further Evidence. *Polymer Journal,* 16(5), 423-429.
Sato, T., & Matsuda, Y. (2009). Macromolecular Assemblies in Solution: Characterization by Light Scattering. *Polymer Journal,* 41(4), 241-251.
Sato, T., Norisuye, T., & Fujita, H. (1984a). Double-Stranded Helix of Xanthan - Dimensional and Hydrodynamic Properties in 0.1-M Aqueous Sodium-Chloride. *Macromolecules,* 17(12), 2696-2700.
Sato, T., Norisuye, T., & Fujita, H. (1984b). Double-Stranded Helix of Xanthan in Dilute-Solution - Evidence from Light-Scattering. *Polymer Journal,* 16(4), 341-350.

Savi, R., de Freitas, R. A., Sassaki, G. L., Koop, H. S., & Silveira, J. L. M. (2015). Real-time monitoring of the change in stiffness of single-strand xanthan gum induced by NaCl. *Food Hydrocolloids,* 44, 191-197.

Shimizu, N., Mori, T., Igarashi, N., Ohta, H., Nagatani, Y., Kosuge, T., & Ito, K. (2013). Refurbishing of Small-Angle X-ray Scattering Beamline, BL-6A at the Photon Factory. *J. Phys.: Conf. Ser.,* 425(20), 202008.

Shimizu, N., Yatabe, K., Nagatani, Y., Saijyo, S., Kosuge, T., & Igarashi, N. (2016). Software development for analysis of small-angle X-ray scattering data. *AIP Conf. Proc.,* 1741(1), 050017.

Stokke, B. T., Elgsaeter, A., & Smidsrod, O. (1986). Electron microscopic study of single-and double-stranded xanthan. *International Journal of Biological Macromolecules,* 8(4), 217-225.

Stokke, B. T., Smidsrød, O., & Elgsaeter, A. (1989). Electron microscopy of native xanthan and xanthan exposed to low ionic strength. *Biopolymers,* 28(2), 617-637.

Teckentrup, J., Al-Hammood, O., Steffens, T., Bednarz, H., Walhorn, V., Niehaus, K., & Anselmetti, D. (2017). Comparative analysis of different xanthan samples by atomic force microscopy. *Journal of Biotechnology,* 257, 2-8.

Tomofuji, Y., Yoshiba, K., Christensen, B. E., & Terao, K. (2019). Single-chain conformation of carboxylated schizophyllan, a triple helical polysaccharide, in dilute alkaline aqueous solution. *Polymer,* 185, 121944.

Yamakawa, H., & Yoshizaki, T. (2016). *Helical Wormlike Chains in Polymer Solutions*. Berlin, Germany: Springer.

Graphical abstract

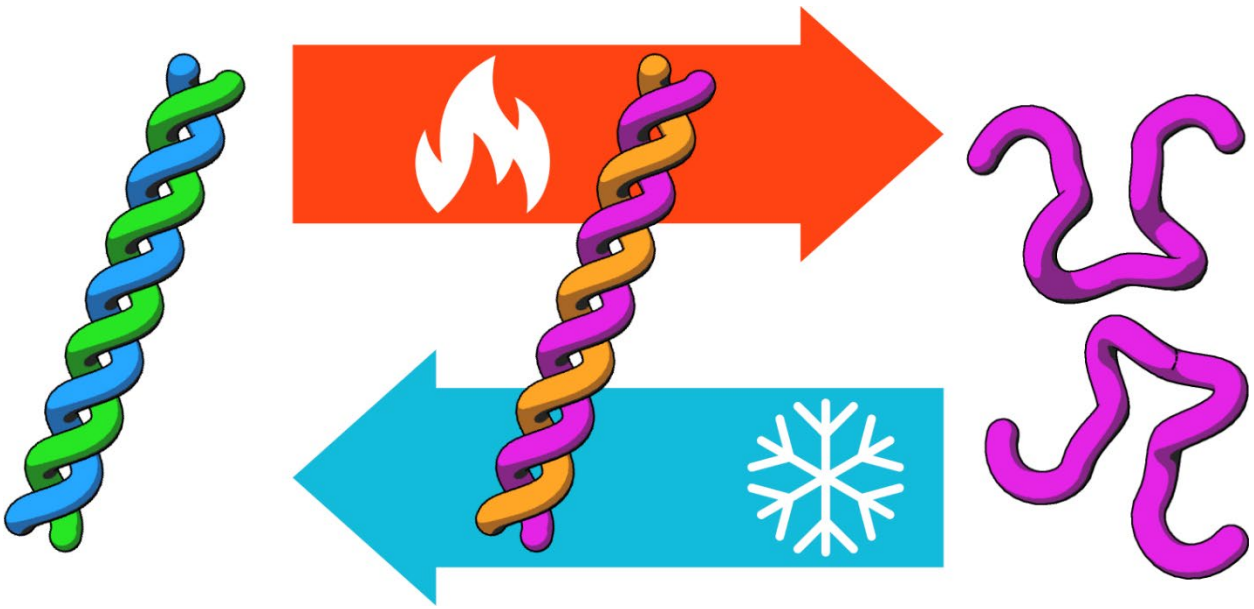

Suppementary materials for

Kinetics of Denaturation and Renaturation Processes of Double-Stranded Helical Polysaccharide, Xanthan in Aqueous Sodium Chloride

Yu Tomofuji[a], Koichi Matsuo[b], and Ken Terao[a,*]

[a]Department of Macromolecular Science, Graduate School of Science, Osaka University, 1-1, Machikaneyama-cho, Toyonaka, Osaka 560-0043, Japan.

[b]Hiroshima Synchrotron Radiation Center, Hiroshima University, Kagamiyama, Higashi-hiroshima, Hiroshima 739-0046, Japan.

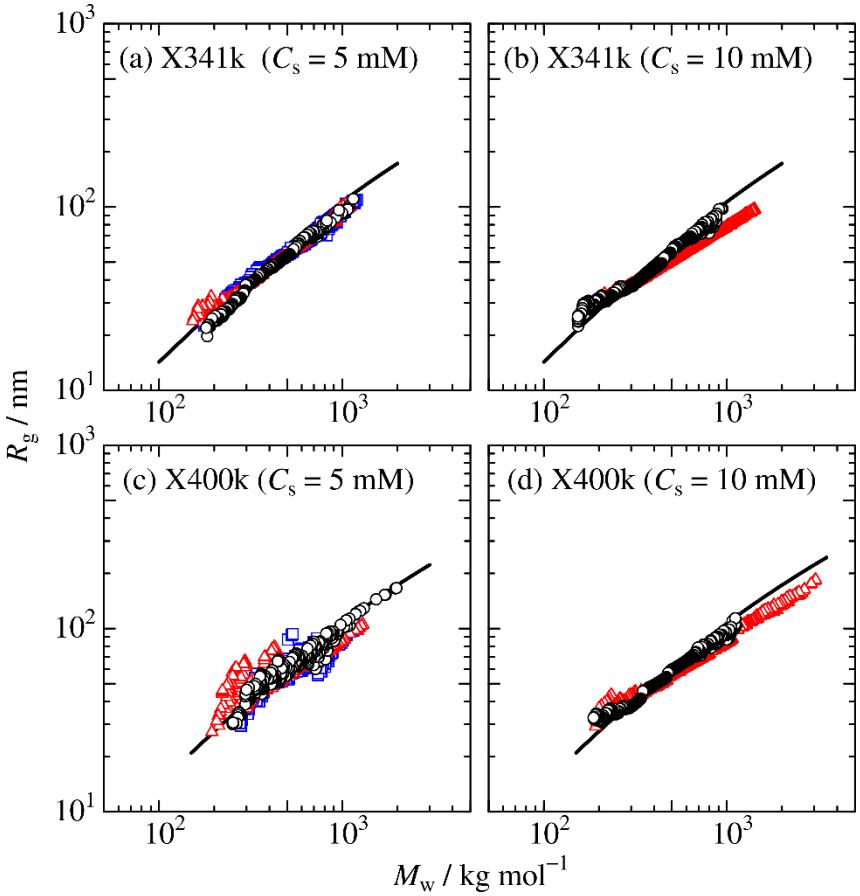

Fig. S1. Weight-average molar mass M_w dependence of the radius of gyration R_g for (a) **X341k** at C_s = 5 mM, (b) **X341k** at C_s = 10 mM, (c) **X400k** at C_s = 5 mM, and (d) **X341k** at C_s = 5 mM. Black circles, blue squares, and red triangles indicate the data for the as-prepared solution, the renatured xanthan sample with c_d = 3.0 – 3.1 mg mL^{-1}, and those with c_d = 5.4 – 6.4 mg mL^{-1}. Solid lines indicate the literature values.[1]

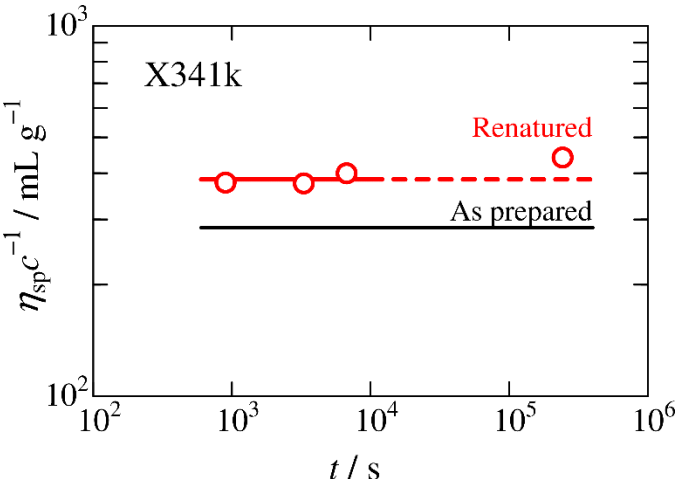

Fig. S2. Specific viscosity η_{sp} plotted against the time t after quenching for **X341k** in 10 mM aqueous NaCl at 20 °C. The denatured (c_d) and measured (c) concentration were 6 mg/mL and 1 mg/mL, respectively.

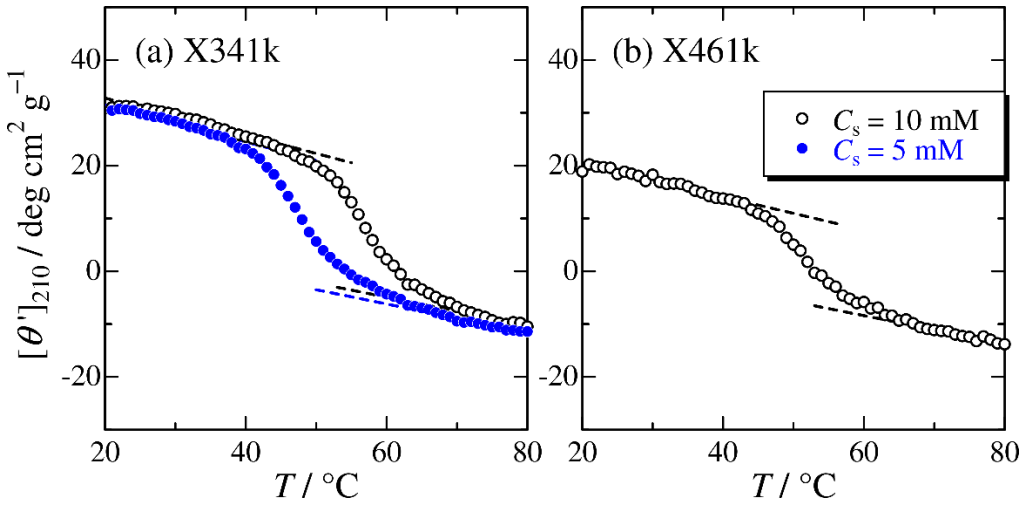

Fig. S3. Temperature dependence of $[\theta']_{210}$ for (a) **X341k** and (b) **X461k** in aqueous NaCl and at λ_0 = 210 nm at indicated C_s. Temperature-raising rate and c were 5 °C min^{-1} and 3 mg mL^{-1}, respectively.

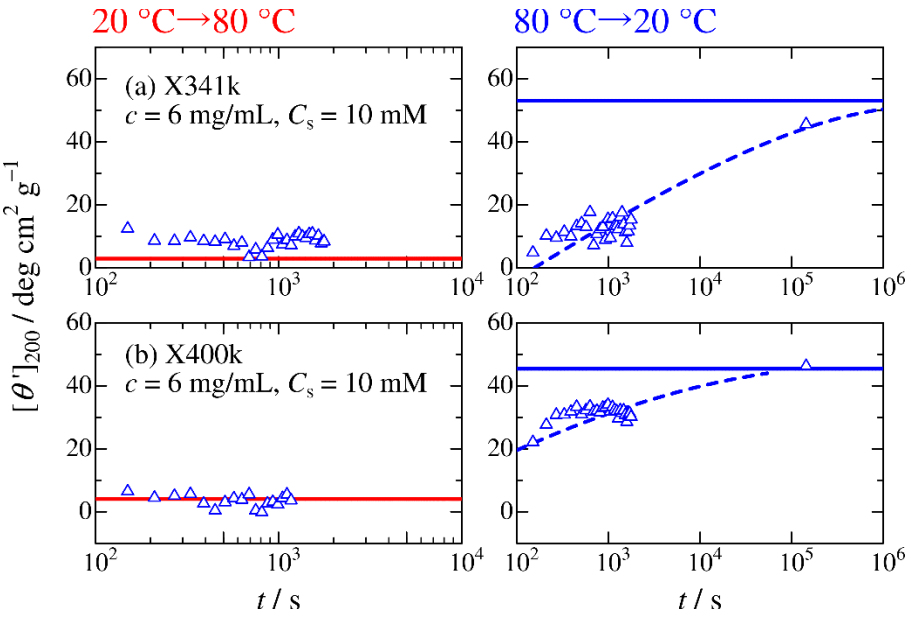

Fig. S4. Time course of $[\theta']_{200}$ for (a) **X341k** and (b) **X400k** in 10 mM aqueous NaCl. Left, abruptly heated from 20 to 80 °C. Right, abruptly cooled from 80 to 20 °C. Solid blue lines, the $[\theta']_{200}$ value for the as-prepared solution at 20 °C.

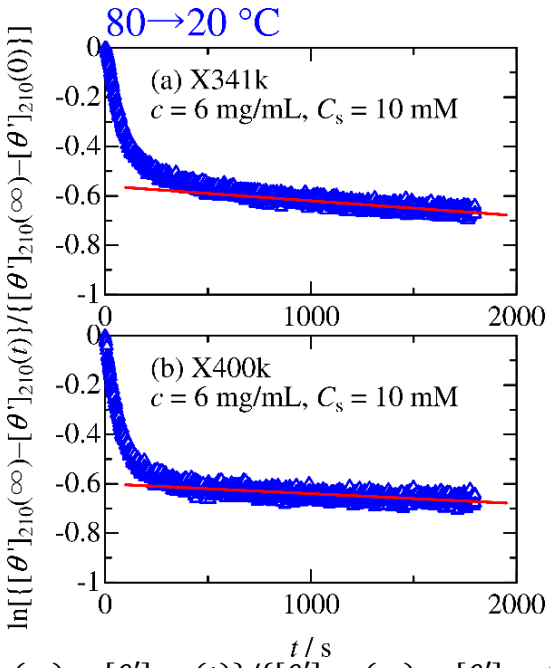

Fig. S5. Plots of $\ln[\{[\theta']_{210}(\infty) - [\theta']_{210}(t)\}/\{[\theta']_{210}(\infty) - [\theta']_{210}(0)\}]$ vs t for (a) **X341k** and (b) **X400k** in 10 mM aqueous NaCl. The first-order rate constant was estimated from the solid red line.

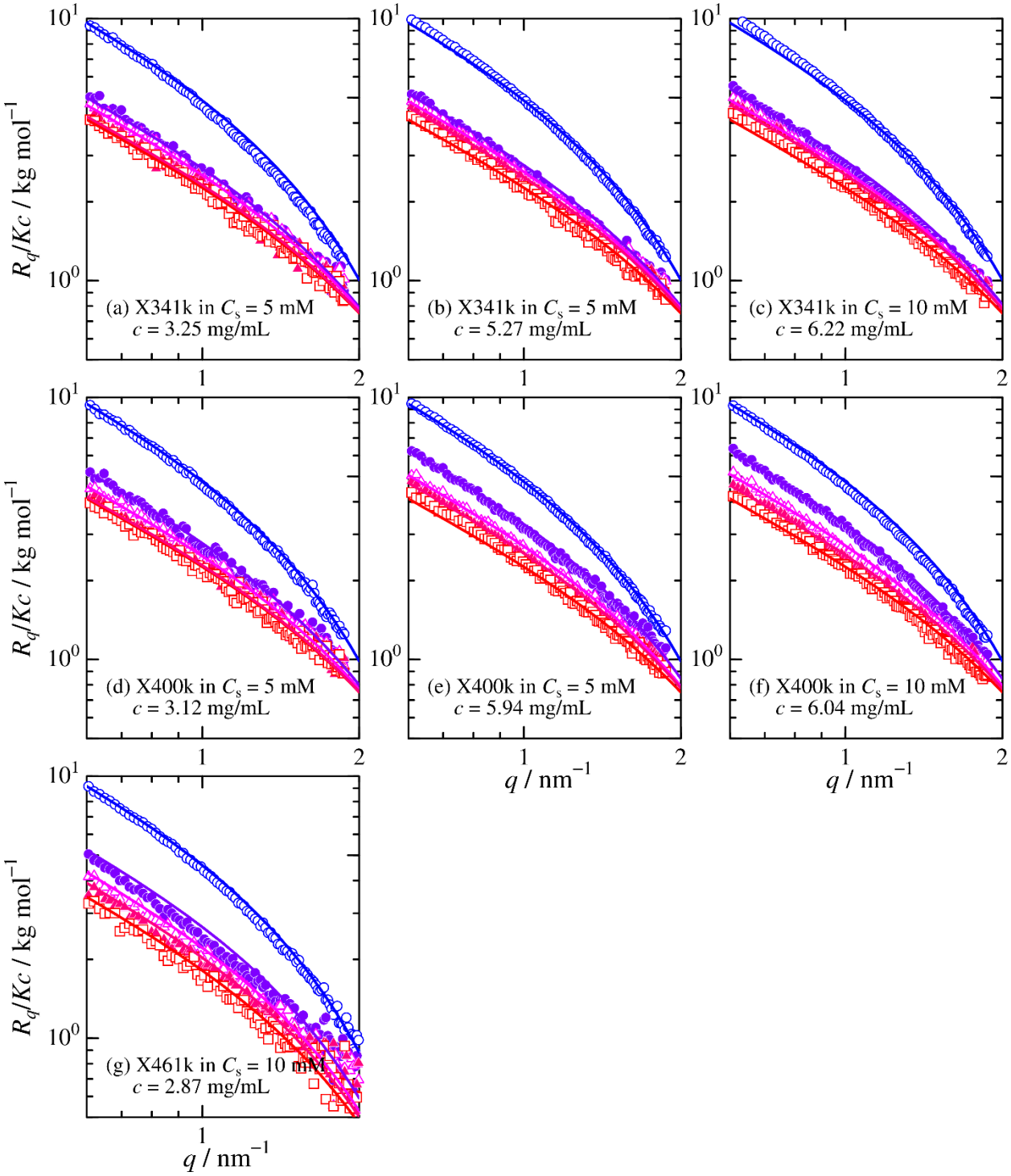

Fig. S6. Enlarge of the middle q region of Fig. 5.

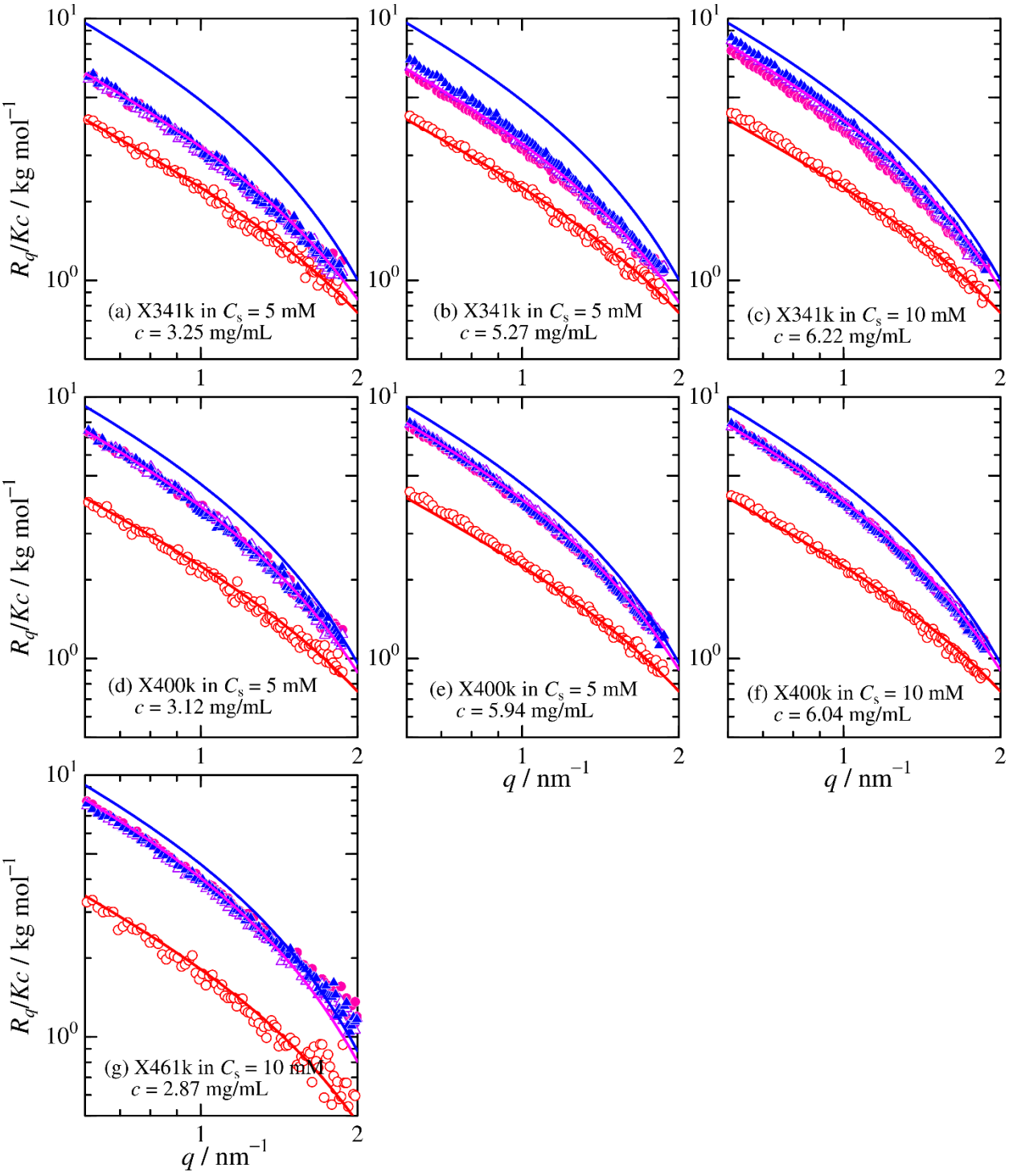

Fig. S7. Enlarge of the middle q region of Fig. 6.

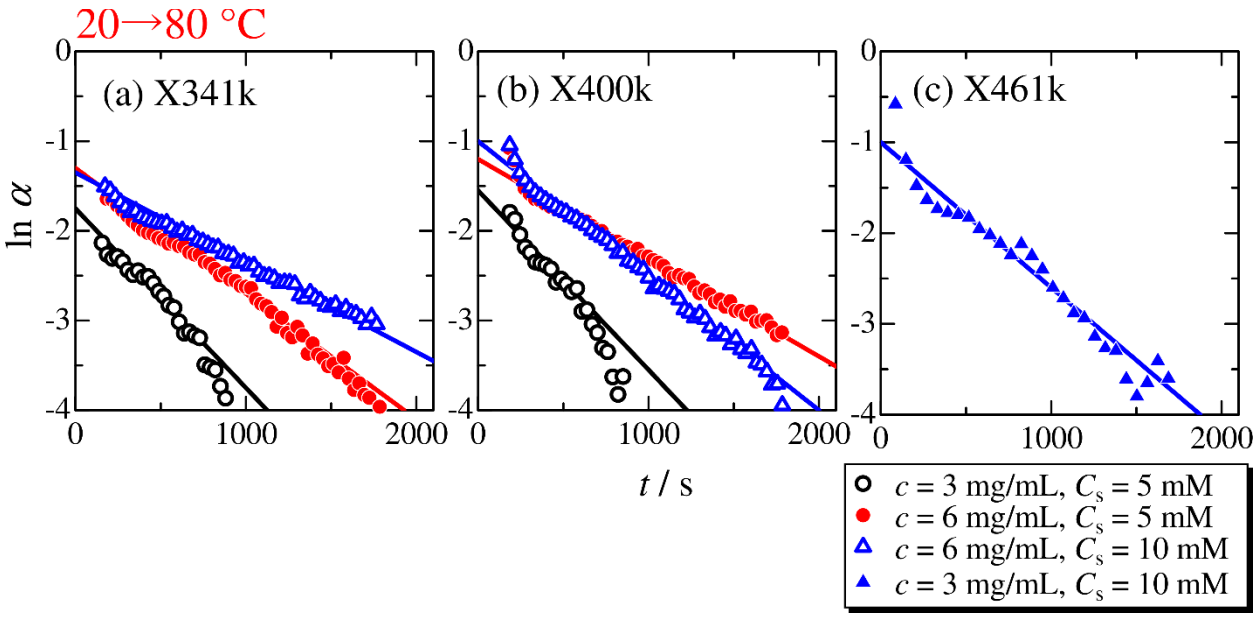

Fig. S8. Plots of lnα vs t for (a) **X341k**, (b) **X400k**, and (c) **X461k** in aqueous NaCl. The first-order rate constant was estimated from the solid lines.

1. Sato, T.; Norisuye, T.; Fujita, H., Double-Stranded Helix of Xanthan - Dimensional and Hydrodynamic Properties in 0.1-M Aqueous Sodium-Chloride. *Macromolecules* **1984,** *17* (12), 2696-2700.